In situ pressure measurement within deformable rectangular polydimethylsiloxane microfluidic devices

Cite as: Biomicrofluidics **6**, 026501 (2012); https://doi.org/10.1063/1.4720394
Submitted: 24 January 2012 • Accepted: 07 May 2012 • Published Online: 18 May 2012

Perry Cheung, Kazumi Toda-Peters and Amy Q. Shen

In situ pressure measurement within deformable rectangular polydimethylsiloxane microfluidic devices

Perry Cheung, Kazumi Toda-Peters, and Amy Q. Shen[a)]
Mechanical Engineering Department, University of Washington, Seattle, Washington 98195, USA

(Received 24 January 2012; accepted 7 May 2012; published online 18 May 2012)

In this paper, we present a simple procedure to incorporate commercially available external pressure transducers into existing microfluidic devices, to monitor pressure-drop in real-time, with minimal design modifications to pre-existing channel designs. We focus on the detailed fabrication steps and assembly to make the process straightforward and robust. The work presented here will benefit those interested in adding pressure drop measurements in polydimethylsiloxane (PDMS) based microchannels without having to modify existing channel designs or requiring additional fabrication steps. By using three different devices with varying aspect ratio channels ($\frac{w}{h_0}$, width/depth), we demonstrate that our approach can easily be adapted into existing channel designs inexpensively. Furthermore, our approach can achieve steady state measurements within a matter of minutes (depending on the fluid) and can easily be used to investigate dynamic pressure drops. In order to validate the accuracy of the measured pressure drops within the three different aspect ratio devices, we compared measured pressure drops of de-ionized water and a 50 wt. % glycerol aqueous solution to four different theoretical expressions. Due to the deformability of PDMS, measured pressure drops were smaller than those predicted by the rigid channel theories (plate and rectangular). Modification of the rigid channel theories with a deformability parameter α provided better fits to the measured data. The elastic rectangular expression developed in this paper does not have a geometric restriction and is better suited for microchannels with a wider range of aspect ratios. © *2012 American Institute of Physics*.
[http://dx.doi.org/10.1063/1.4720394]

I. INTRODUCTION

The ability to control and analyze the flow of fluids in microfluidic devices is important for developing tools in lab-on-chip devices.[1–9] For instance, pressure drop measurements within microfluidic channels can greatly aid in designing passive microfluidic pumps,[3,4] obtaining rheological properties in microfluidic rheometers,[5,9] and measuring the mechanical properties of biological materials.[6,7]

Several research groups[10–12] have used silicon based microchannels because silicon can be routinely etched to incorporate various sensing elements. The pressure drop measurement with silicon based microdevice involves reflecting an imposed laser beam upon a deflecting silicon channel wall and relating the reflection angle to the channel pressure.[10] Although silicon is a great material to precisely fabricate microfluidic devices, some of its largest drawbacks are its high cost, long and possibly complicated fabrication steps, and its lack of optical transparency.

Alternatively, polydimethylsiloxane (PDMS) based microchannels bonded to glass substrates are commonly used because the same fabrication technology is utilized as silicon microchannels, but at significantly reduced time and cost. Additionally, PDMS is optically transparent, hence allows straightforward visualization of the devices. Recently, several research

[a)]Author to whom correspondence should be addressed. Electronic mail: amyshen@uw.edu.

groups[6,13–17] have used the elastic nature of PDMS as a tool to relate the channel pressure from the deflection of the PDMS wall by using imaging tools such as microscopes. However, these methods often require multiple fabrication steps[14] to incorporate additional channel layers onto the main PDMS flow channel,[6,13,15,16] fluorescent particles,[6,17] or even introduce separate probing fluids.[13,15]

In order to afford the flexibility of measuring pressure drops in existing PDMS microdevices with minimal alterations, a straightforward and repeatable method is necessary. The careful incorporation of external pressure transducers[1,3–5,9] satisfies this requirement, since it requires only an external sensor that is not uniquely associated with any design or microfluidic device. Furthermore, pressure transducers can provide real-time dynamic pressure measurements since they can easily be coupled to high-speed data acquisition hardware.

The existing pressure versus flow rate relationship is based on the assumption that the channel walls are rigid. By solving the Navier-Stokes equation for a fully developed, steady-state flow with a Newtonian fluid between *parallel rigid plates* (equivalent to a rectangular channel with channel width w $\gg$ height h),[1] the pressure drop across microchannel length L is represented by

$$\Delta p = Q\frac{12\mu L}{h^3 w}, \tag{1}$$

where Δp is the pressure drop across a channel length L, Q is the imposed flow rate, h is the height of the microchannel, and μ is the kinematic viscosity of the Newtonian fluid. We denote Eq. (1) as *rigid plate expression*.

Using an elastic polymer based substrate such as PDMS adds additional complexity due to the channel's ability to deform during flow. Realizing the dependence of flow rate on cross sectional area and therefore the dependence of pressure drop on cross sectional area, the rigid walled channel assumption (see Eq. (1)) would lead to the predicted pressure much higher than what is actually present when the cross section is allowed to deform. Gervais *et al.*[1] recently proposed to take into account the cross sectional deformation of high aspect ratio (channel width/channel height) PDMS microchannels due to pressure-driven flow of a fluid. They assumed that the pressure was not only a function of flow rate but also of position along the channel direction z

$$-\frac{dp(z)}{dz} = Q\frac{12\mu}{h(z)^3 w}, \tag{2}$$

where z is the stream-wise axis and $p(z)$ is the stream-wise variation in pressure due to the stream-wise variation in the microchannel height, $h(z)$. In order to account for the deformation in the channel, scaling approximations assuming Hooke's law were performed by Gervais *et al.*[1] to relate the vertical and lateral strains to the deformation of the channel height over channel width and the deformation of the channel width over the channel height, respectively. Both the vertical and lateral strains were also scaled to the pressure in the channel over Young's modulus (E). Based on physical arguments, the lateral deformation involving the channel wall was neglected for the case where $w \gg h$ and only deformations of the channel height were deemed significant. At any position z, the relative maximum thickness variation inside the channel can then be inferred to be

$$\frac{\Delta h_{max}}{h_0} = c_1\frac{pw}{Eh_0}, \tag{3}$$

where Δh_{max} is the maximum height increase at mid width of the channel under deformation, h_0 is the channel's original height, and c_1 is a dimensionless proportionality constant. Note that when the channel's aspect ratio is close to 1, the scaling law of Eq. (3) still holds but the deformation would occur on the three PDMS walls assuming the other substrate is glass. However, it was argued that given the Young's modulus for PDMS being on the order of 10 atm, the entire

channel is unlikely to deform even when $w \sim h$, especially when pressure above 2 atm leads to the external fluidic connections to leak. Thus, the use of Eq. (3) for qualitative predictions was considered to be relevant even for channels with aspect ratios close to 1. By using a width-averaged displacement $\langle \Delta h \rangle$, an effective channel height at any distance z could be described by

$$h(z) = h_0 \left(1 + \frac{\langle \Delta h \rangle}{h_0} \right). \tag{4}$$

If the deflection of the PDMS wall is small and the shape of the deforming wall was assumed to be parabolic, then $\langle \Delta h \rangle \sim \frac{2}{3} \Delta h_{max}$. By combining Eqs. (3) and (4), the effective channel height can be expressed as

$$h(z) = h_0 \left(1 + \alpha \frac{p(z) w}{E h_0} \right), \tag{5}$$

where $\alpha = \frac{2}{3} c_1$. Physically, α represents a dimensionless deformability factor and when α approaches zero, the channel approaches a rigid structure, and the channel height $h(z)$ becomes a constant h_0. Combining Eqs. (2) and (5) results in

$$-\frac{dp(z)}{dz} = Q \frac{12\mu}{h_0^3 w} \left(1 + \alpha \frac{p(z) w}{E h_0} \right)^{-3}. \tag{6}$$

Equation (6) relates the differential pressure drop to flow-rate accounting for the channel height variation due to substrate deformation during the flow. Integrating Eq. (6) with respect to stream-wise position and with the outlet condition $p(z = L) \equiv 0$ results in

$$Q = \frac{h_0^4 E}{48 \alpha \mu (L - z)} \left[\left(1 + \alpha \frac{p(z) w}{E h_0} \right)^4 - 1 \right]. \tag{7}$$

For an elastic plate geometry, Eq. (7) describes how the microchannel pressure varies along stream wise position z for an imposed flow rate Q. For future references, we denote Eq. (1) as *rigid plate* expression and Eq. (7) as *elastic plate* expression.

Gervais *et al.*[1] validated their elastic plate expression (Eq. (7)) using a combination of imaging the deflection of the PDMS wall and pressure-drop measurements with two relatively high aspect ratio ($w/h_0 = 10$ and 20) cases in PDMS microchannels bonded to glass substrates, under imposed flow-rates. For each PDMS microchannel, their measured pressure drop data laid below the rigid plate expression prediction. The deviation from the rigid plate expression increased with increasing channel width at fixed channel height. A good best-fit (about 75% of the data fell on the curve) to the measured data was achieved for each microchannel when elastic plate expression (Eq. (7)) was plotted against the measured data with the deformability factor α as a fitting parameter.

Based on physical reasoning, α should decrease as Young's modulus E increased (i.e., closer to rigid channel walls) to keep this deformability factor valid and bound. Also, it would be reasonable to expect α to decrease as the channel width decreases for a fixed channel height since the total deflection would decrease with less channel width. Based on their reported α values, Gervais *et al.* indeed observed a drop in α as the Young's modulus increased (for channels with the same dimensions).

Based on the work of Gervais *et al.*,[1] we further explore the deformability factor α in elastic microfluidic channels in this paper. Depending on the application the aspect ratio of PDMS microchannels can be near unity,[3,18–22] for example, square microchannels are commonly used to control both the size and formation of droplets for materials synthesis and lab on chip analyses.[19,22] Hence, we need an alternative Eq. (7) to relate the pressure drop and flow rate for aspect ratios close to unity. Here, we develop a new pressure drop versus flow-rate expression for

deformable rectangular channels with wider range of aspect ratios. We also describe a straightforward procedure to incorporate commercially available pressure transducers within PDMS microfluidic channels to monitor pressure-drop in real-time. This process is relatively inexpensive and requires minimal design modifications to pre-existing channel designs.

A. Theoretical background

For a rigid rectangular channel cross section and assuming the upper limit of the aspect ratio $w/h \sim 1$, a fully developed, steady-state Newtonian flow can be described by solving the Navier-Stokes equation, using Fourier sum representation, the approximate solution (within 10% error[23]) can be expressed as

$$\Delta p = \frac{Q}{h^3 w} \frac{12\mu L}{\left(1 - 0.63\frac{h}{w}\right)}. \tag{8}$$

To account for channel deformation during flow, we adopt a similar approach used by Gervais *et al.*,[1] assuming the PDMS top wall deforms with a parabolic cross section, inserting Eq. (5) into Eq. (8)

$$-\frac{dp(z)}{dz} = Q \frac{12\mu}{\left[1 - 0.63\frac{h_0}{w}\left(1 + \frac{\alpha p(z) w}{E h_0}\right)\right]} \frac{1}{h_0^3 w \left(1 + \frac{\alpha p(z) w}{E h_0}\right)^3}. \tag{9}$$

Integrating Eq. (9) with respect to stream-wise position z and with the outlet condition $p(z = L) \equiv 0$ yields the relationship for an elastic rectangular cross-section

$$Q = \frac{h_0^4 E}{48\alpha\mu(L - z)} \left\{ \left[\left(1 + \alpha \frac{p(z) w}{E h_0}\right)^4 - 1 \right] - 0.504 \frac{h_0}{w} \left[\left(1 + \alpha \frac{p(z) w}{E h_0}\right)^5 - 1 \right] \right\}. \tag{10}$$

For future references, we denote Eq. (8) as *rigid rectangular* expression and Eq. (10) as *elastic rectangular* expression.

II. METHODS AND MATERIALS

A. Pressure transducer

The PX26-005DV pressure transducer was chosen for the small size (~35 mm in length and ~10 mm in diameter), low weight, and possessing a wide differential pressure range of 0-34.47 kPa (Omega Engineering, Inc., Stamford, CT). A calibration curve was obtained by applying known hydrostatic heads on one end of the pressure transducer and measuring the resulting voltage output. The calibration curve was subsequently used to relate the measured voltage output to a differential pressure drop measurement at various applied flow rates.

B. Device design

The method proposed here is intended to adapt existing microfluidic designs to accept an *in situ* pressure metering system (i.e., pressure transducers) with minimal alterations, as shown in Figure 1. A pair of transducer channels (iii) leading from the main flow channel (ii) is added to provide a fluidic connection to the external pressure transducer via the transducer ports (iv) while a given fluid flows through the main flow channel via inlet/outlet ports (i). Specific dimensions for the three devices A, B, and C with varying aspect ratios are shown in Table I.

C. Device fabrication

Single layer soft lithography[24] was used to create a master mold on a clean silicon substrate. SU-8 2002 (MicroChem Corp., Newton, MA) was spin coated at a speed of 2250 RPM

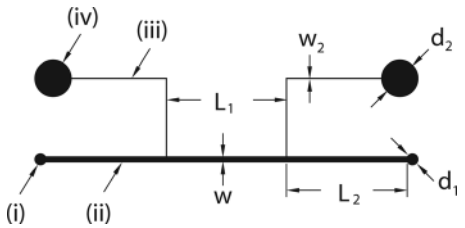

FIG. 1. A schematic of the channel design used, showing the (i) main channel inlet/outlet ports, (ii) main flow channel, (iii) transducer channels, (iv) transducer inlet/outlet ports.

initially before spin coating SU8-2100 (MicroChem Corp., Newton, MA) at 2250 RPM to set the final thickness to ∼96 μm for devices B and C and ∼70 μm for device A. The SU-8 coated substrates were exposed with a Heildelberg μPg 101 laser pattern generator (Heildelberg Instruments GmbH, Heildelberg, Germany).

The PDMS channels were created using a two part Sylgard 184 PDMS polymer kit (Dow Corning, Midland, MI), mixed to a ratio of 10:1 (pre-polymer:cross-linker). The mixed PDMS was allowed to degas under vacuum in a desiccator for an hour. Figure 2 shows the external components of the devices. Before the PDMS mixture was poured over the silicon master, all inlet and outlet ports (iii) and (vi) were fastened to the wafer using model glue (The Testor Corp, Rockford, IL). Both the main channel ports (vi) and transducer ports (iii) were composed of silicone tubing 0.76 mm I.D. and 2.79 mm I.D. respectively (Cole-Parmer Instrument Company, Vernon Hills, IL). Once the ports were in place, the PDMS mixture was poured over the master, placed under vacuum in the desiccator to remove excess air bubbles, and then cured in a 65 °C oven for an hour. Referring to Figure 2, once the PDMS layer (ii) was fully cured, it was cut and peeled from the silicon master and bonded using a Femto plasma cleaner (Diener Electronic, Reading, PA) to a glass microscope slide (i) to complete the device fabrication. Flow was directed to and from the device via polyethylene 0.38 mm I.D. tubing (Becton Dickinson, Sparks, MD) connected to the main channel ports (not shown).

Once the device is assembled with the transducer port (iii), 12 gauge polytetrafluoroethylene (PTFE) linking-tubing (iv) (Zeus, Inc., Orangeberg, SC), and silicone transducer tubing (v) (Cole-Parmer Instrument Company, Vernon Hills, IL), the fluid of interest was pumped into the device through the main channel ports (vi) until the liquid-air interface emerged at the transducer tubing. To prevent loss of fluid during the filling, clamps were placed at the transducer tubing and outlet channel port to direct the flow. The pressure transducer (iv) was then carefully filled with the fluid using a syringe and needle until the liquid-air interface filled up each transducer port. Care was taken to position the needle close to the transducer diaphragm without puncturing. The pressure transducer was then carefully inserted into the transducer tubing such that the liquid-air interfaces merged, and air bubbles were avoided. It was extremely important to make sure all the connections from the flow device to the pressure transducer were

TABLE I. Important dimensions for the three devices (see Figure 1 for reference).

Device	A	B	C
w (μm)	1000	500	200
h_0 (μm)	68	97	97
w/h_0	14.7	5.2	2.1
w_2 (μm)	200	200	200
L_1 (mm)	20	20	20
L_2 (mm)	20	10	4
d_1 (mm)	6	6	6
d_1 (mm)	2	2	2

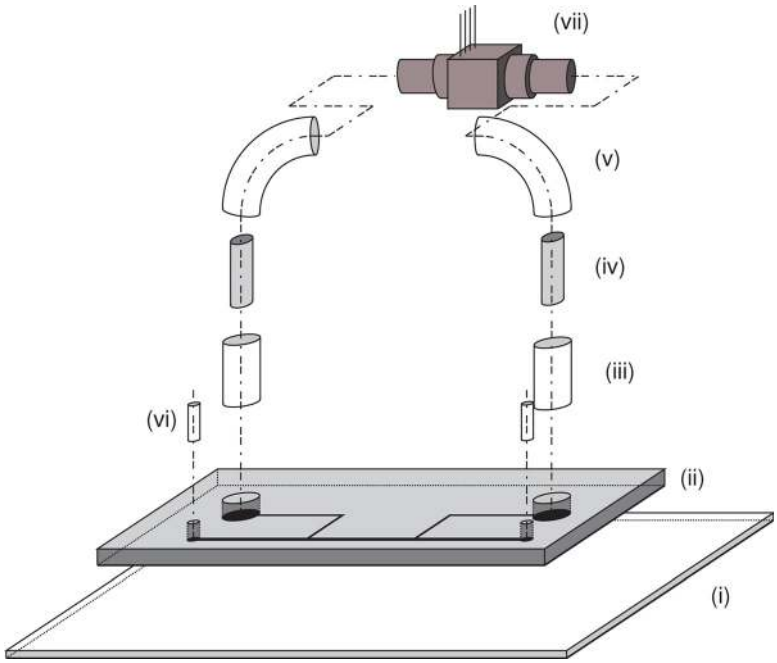

FIG. 2. A detailed schematic showing the various external components to the microfluidic device: (i) glass slide, (ii) PDMS layer, (iii) transducer port, (iv) linking tube, (v) transducer tubing, (vi) main channel port, (vii) pressure transducer.

completely filled with the working fluid to avoid air bubbles. Any air bubble present that spans the width of the tubing will provide an additional pressure offset due to capillarity. If this occurred, the tubes were purged and refilled with the working fluid until all air bubbles were removed. The PTFE linking-tube (iv) was used to make this filling and purging effort easier. The use of these external tubing connections allows for quick interchanging of different pressure transducers and easy adapting of various channel designs.

D. Pressure drop measurements

Two fluids, de-ionized (DI) water and a 50 wt. % glycerol solution, were chosen to test the accuracy of the pressure metering system. The DI water was placed in a Branson 2510 sonicator (Branson Ultrasonics Corp, Danbury, CT) and degassed by vacuum aspiration for 1 h before use. The degassing of the working fluids reduces the chance for trapping air bubbles during assembly of the device. The glycerol solution was used to achieve higher pressure drops due to its high viscosity when compared to water. Glycerol (Mallinckrodt Baker, Inc., Phillipsberg, NJ) was mixed with water in equal parts by weight (50 wt. %) to achieve a viscosity of 5–6 times larger than that of water.[25] Due to the hygroscopic nature of glycerol, new batches were made and the viscosity was measured before every use. The zero shear viscosity of the DI water and glycerol solution was measured using an AR 2000 rheometer (TA Instruments, New Castle, DE) fitted with a 40 mm 2° acrylic cone and plate geometry.

All flow tests were performed using a 50 ml model 1050TTL glass gas tight syringe (Hamilton Company, Reno, NV). Glass syringes were used because they have a quicker response time over disposable plastic syringes and led to less pressure fluctuations from syringe flexing. Further reduction in pressure fluctuations could be achieved, if necessary, by minimizing the tubing between the pressure transducer and the transducer port. The flow rate was controlled with an original equipment manufacturer (OEM) high pressure syringe pump module 702202 (Harvard Apparatus, Holliston, MS). Data acquisition was conducted with a NI PCI 6221 M Series DAQ card (National Instruments, Austin, TX) and processed via a custom built LabVIEW program (LabVIEW 2010). Pressure drop measurements were recorded upon reaching steady state. The Reynolds numbers range from 0.049 to 188 in this work, depending on the

given flow rate, channel geometry, and the fluid's viscosities. More information on the Reynolds number is enclosed in the captions of Figures 4 and 5.

Figure 3 shows examples of the dynamic pressure drop upon a change in flow-rate for both DI water and the 50 wt. % glycerol solution. Steady state pressure drop was typically achieved within 30–90 s using DI water and within 1–5 min using the glycerol solution. Although not presented here, this approach could be used to monitor any dynamic changes in the pressure drop, for example, the non-steady flow in channels during droplet production.[3,19,22] The resolution of dynamic pressure measurements is limited by the sampling rate of the data acquisition card, response time of the pressure transducers, and signal-noise from vibrations and flexing of flexible components. For all the works presented here, the flow of fluids is continuous and individual steady state (i.e., steady flow) measurements are completed within minutes, so evaporation of water and any gas diffusion into the channels and its affects are negligible. Gas diffusion only becomes an issue when flow is stopped and the fluid within the channels is allowed to evaporate (on the order of several hours depending on the thickness of the PDMS).[26,27] If significant evaporation has occurred and gas bubbles are clearly visible within the channels, the fluidic connections can be disassembled and the channel and pressure transducers can be placed back in the vacuum aspirator for degassing.

III. RESULTS AND DISCUSSION

Figures 4(a)–4(c) show the steady state pressure drop versus flow-rate for DI water in devices A, B, and C, respectively. Figures 5(a)–5(c) show the steady state pressure drop versus flow-rate for the 50 wt. % glycerol solution through devices A, B, and C, respectively. For each figure, the experimental data (•) is plotted against the rigid rectangular channel (– – – – – –), rigid plate (——·——), elastic rectangular channel (— — —), and elastic plate (———) curves.

Recall that the rigid rectangular channel and rigid plate curves were calculated from Eqs. (8) and (1), respectively. The elastic rectangular channel and elastic plate curves were determined by curve-fitting Eqs. (10) and (7) to the measured data, respectively. Using the dimensionless deformability factor α as the only fitting parameter, the root mean squared error between the imposed flow-rate and the predicted flow-rate at a given measured pressure drop was minimized. A constant value of 2.2 MPa was chosen for the Young's modulus[28] based on our PDMS mixing ratio and curing time. The best-fit α values are tabulated in Table II for each device and fluid used.

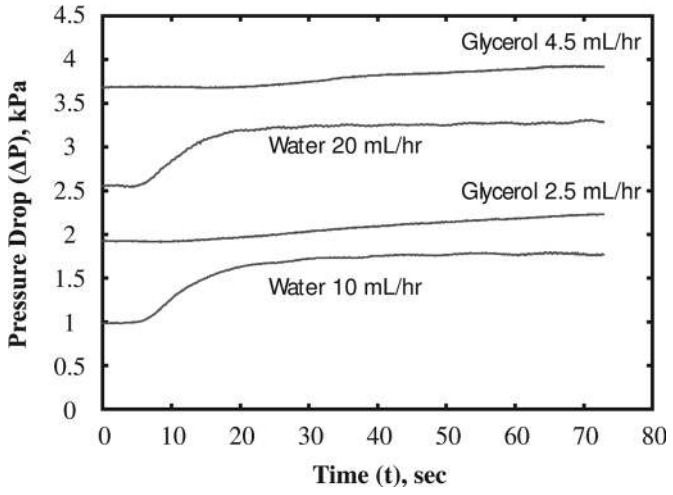

FIG. 3. Examples of dynamic pressure drop measurements upon a change in flow-rate using DI water and the 50 wt. % glycerol solution within device A. Steady state for DI water and 50 wt. % glycerol solution was achieved after ~30 s and ~70 s, respectively.

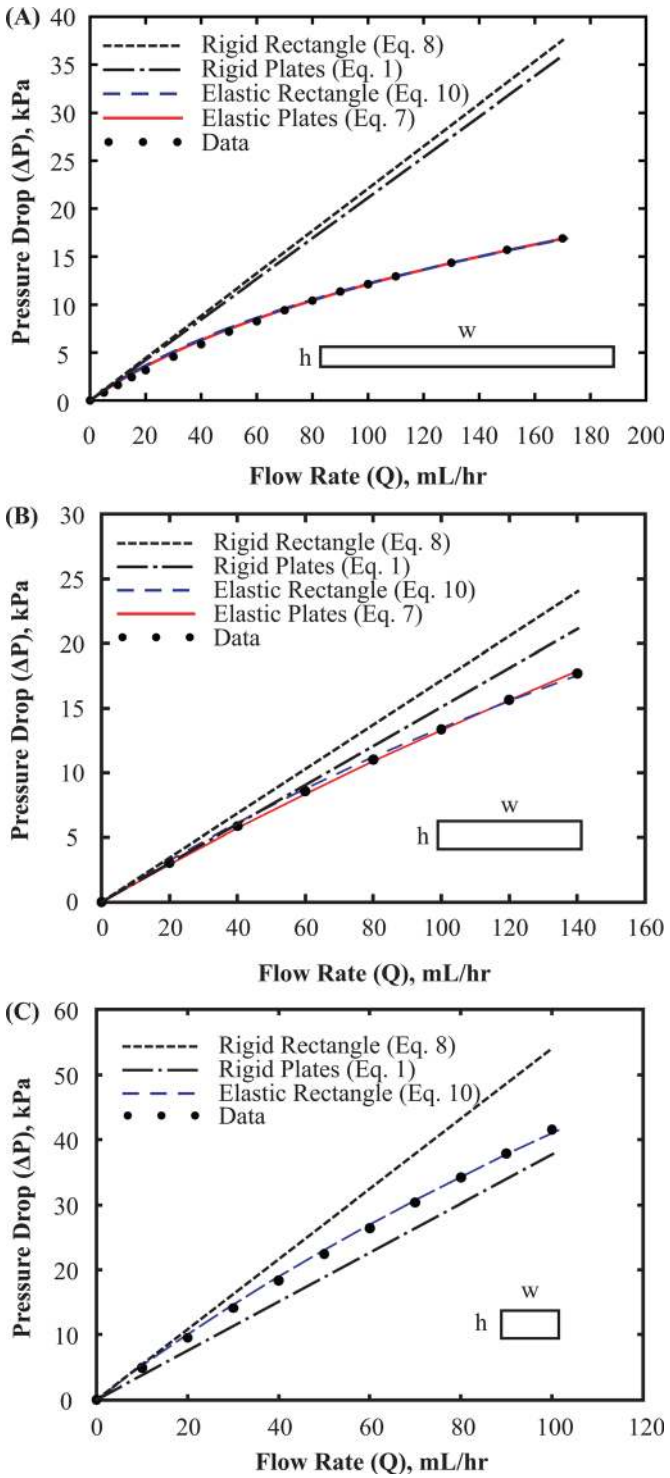

FIG. 4. Pressure drop vs. flow-rate data (dot) and analytic expressions (lines) for DI water. (a) Device A, Re $\sim (2.61, 88.9)$, (b) device B, Re $\sim (17.9, 130)$, (c) device C, Re $\sim (18.9, 188)$.

In Figure 4(a) (high aspect ratio, $w/h_0 = 14.7$), we see that neither of the rigid channel theories (Eqs. (1) and (8)) accurately describe the pressure drop in the channel beyond low pressure-drops ($p < 2$ kPa) but rather predicts a higher pressure-drop compared to the measured data. From the experiments performed on device A (Figure 4(a)), the non-linear deviation from

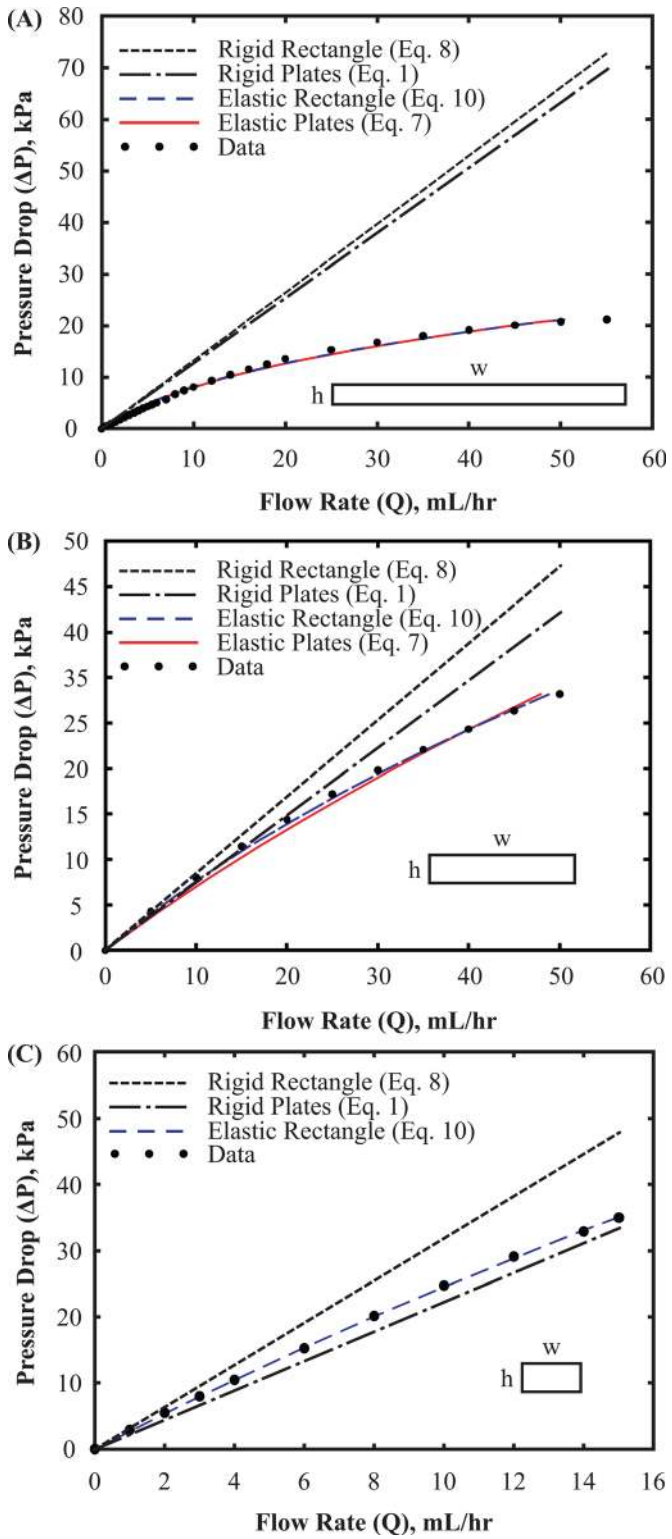

FIG. 5. Pressure drop vs. flow-rate data (dot) and analytic expressions (lines) for a 50 wt. % glycerol solution (a) device A, $\mathrm{Re} \sim (0.049, 5.39)$, (b) device B, $\mathrm{Re} \sim (1.06, 10.6)$, (c) device C, $\mathrm{Re} \sim (0.412, 6.17)$.

TABLE II. Best-fit α values for each device for both DI water and the 50 wt. % glycerol solution.

Device	A	B	C
α_{plate} (water)	4.83	2.66	N/A
α_{plate} (glycerol)	5.76	2.37	N/A
α_{rec} (water)	5.29	5.39	5.79
α_{rec} (glycerol)	6.20	4.15	3.98

the rigid channel theories during flow can be accurately described by both elastic plate and elastic rectangular theories using the best-fit values of α. The good fit to the elastic theories validate the assumptions presented by Gervais *et al.*,[1] where bulging of the PDMS microchannels leads to increase in the cross sectional area, resulting in an overall lower pressure drop.

Figure 4(b) (mid aspect ratio, $w/h_0 = 5.2$) also shows a non-linear deviation of measured data from the rigid channel theories, but to a lesser degree compared to Figure 4(a). The pressure drop data remain linear and seem to behave like a rigid parallel plate microchannel at low pressures (<5 kPa). Both elastic theories appear to fit this device's behavior well. Due to the lower aspect ratio compared to device A, the top wall of the microchannel is not able to deform as much, which results in the data predicted closer by the rigid channel theories.

The data from Figure 4(c) (low aspect ratio, $w/h_0 = 2.1$) show measured pressure drops laying above the rigid parallel plate expression and below that of the rigid rectangular channel expression. The rigid parallel plate expression (Eq. (1)) fails to fit the data even at low flow rates because the assumption for parallel plates breaks down at the given low aspect ratio of device C. Furthermore, the elastic plate expression (Eq. (7)), which is originally derived from the rigid parallel plate expression (Eq. (1)), also naturally fails when the assumption for parallel plates breaks down. Since α is a dimensionless deformability factor, a decrease in α would only result in effectively decreasing the channel cross-section, which then leads to an increase in the elastic plate pressure versus flow rate curve. Thus, the elastic plate expression (Eq. (7)) is not shown in Figure 4(c) because the maximum pressure versus flow rate curve that can be achieved is when α is reduced to zero (i.e., equivalent to Eq. (1)). Observing Figure 4(c), when the aspect ratio is near unity, the elastic rectangle expression provides a very good fit to the experimental data.

Due to the dependence of viscosity on pressure drop measurements, we also tested the accuracy of the elastic theories on a Newtonian fluid with a higher viscosity (50 wt. % glycerol solution). Additionally, the glycerol solution reached higher pressure-drops at lower flow-rates when compared to those of DI water. The data in Figure 5(a) (high aspect ratio, $w/h_0 = 14.7$) show large deviations from the rigid channel theories. At high flow-rates (>45 ml/h), the measured pressure drop increases at a much lower rate. Both elastic channel theories fit the data well with the appropriate α values.

Similar to Figure 4(b), the data in Figure 5(b) (mid aspect ratio, $w/h_0 = 5.2$) show a slight deviation from both rigid channel theories. Similarly, both elastic theories provide good fits to the data. The decreased deviation from rigid theories, when compared with Figure 5(a), is a result from the decreased channel width which decreases the deformability of the channel.

As expected, the data obtained from glycerol experiments performed on device C (low aspect ratio, $w/h_0 = 2.1$) (Figure 5(c)) show pressure-drops lie above the rigid plate expression and below the rigid rectangle expression. Since the aspect ratio is closer to unity, the parallel plate assumption is no longer valid, only the rectangular channel theories are appropriate. Clearly, the elastic rectangular expression fits the data very well. Similar to Figure 4(c), the elastic plate expression is not shown since the maximum pressure versus flow rate curve that can be achieved by varying α is equivalent to the rigid plate expression and the parallel plate assumption is no longer valid.

By examining the best-fit α values obtained from elastic plate expression in Table II, we observe a drop in α_{plate} as the aspect ratio (w/h_0) decreases (i.e., A has the highest aspect ratio)

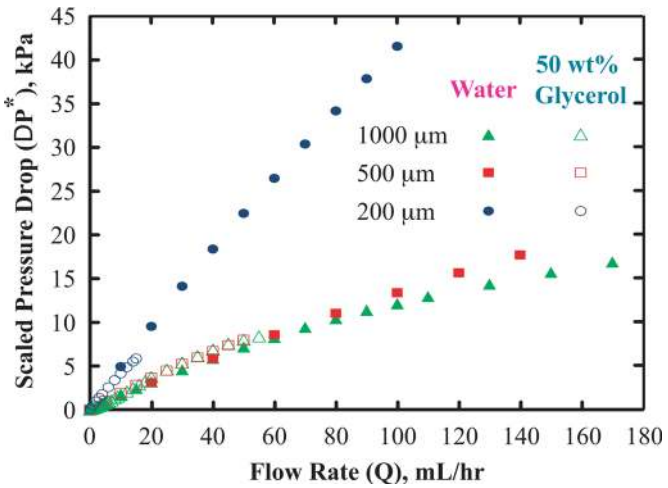

FIG. 6. Scaled pressure drop measurements versus flow-rate data for both the DI water (filled symbols) and the 50 wt. % glycerol solution (open symbols) for all three device dimensions (1000 μm, 500 μm, and 200 μm).

for both solutions. When we use the elastic rectangular expression developed in this paper, we observe a drop in α_{rec} with the 50 wt. % glycerol solution with decreasing aspect ratio and an almost constant α_{rec} with DI water. The constant α, simply reflects the precision of the α value to be within $\pm\sim$0.5 from the best-fitting. Nonetheless, we still observe a consistent and expected trend in a lower α with decreasing channel width for the 50 wt. % glycerol solution using both elastic theories.

A direct comparison of the best-fit α values between DI water and the 50 wt. % glycerol solution within a single device, as tabulated in Table II, may appear that the best-fits are required for each fluid and not just dependent on the channel dimensions. This apparent shortcoming is due entirely to the scaling effect by the more viscous 50 wt. % glycerol solution. When the measured pressure drop of the 50 wt. % glycerol solution is normalized by its viscosity with the viscosity of DI water as the reference, the resulting scaled pressure drop (ΔP^*) in Fig. 6 shows the glycerol data lay on the DI water data for each device dimension. Thus, the viscosity of the fluids used has a slight scaling effect on the best-fit α values obtained, but the approach described here shows that the measured pressure drops are self-consistent and that channel deformation is dependent only on the Young's modulus of the PDMS substrate and channel aspect ratio. Since α was originally derived from scaling relations to circumvent numerically solving a series of coupled differential equations, the exact value of α cannot be determined easily based on channel dimensions or material properties without actually performing fluid-materials structure computations.[1] Gervais *et al.*[1]note that the simulations reveal the value of α remains approximately constant for a given geometry. When we compare the best fit α values in Table II for each device (i.e., same geometry) for both the plate and rectangular theories, we find that the α values are fairly consistent within each device.

Finally, we would like to point out that our experimental setup enables the direct measurement of pressure drop within a microchannel with varying microchannel aspect ratios and PDMS modulus for any given flow rate. The elastic rectangular expression and the deformability factor α presented in this paper merely provide a theoretical basis to verify and validate our pressure drop measurements with respect to varying microchannel geometry and flow rates. Experimentally, we do not need to determine the deformability factor α to obtain the pressure readings.

IV. CONCLUSION

Pressure drop measurements in PDMS channels bonded to glass substrates are difficult and expensive to set up because it usually relies on measuring the deformation of PDMS walls by

using imaging techniques. In this work, we proposed a simple procedure to incorporate external pressure transducers into existing microfluidic devices to make the process straightforward and robust by using a series of interchangeable tubing. Additionally, we have demonstrated that our approach can easily be adapted into existing channel designs by using three different devices with varying aspect ratio channels. Furthermore, our approach can achieve steady state measurements within a matter of minutes (depending on the fluid) and can easily be used to investigate dynamic pressure drops. In order to validate the accuracy of the measured pressure drops within the three channels, we compared measured pressure drop with several analytic expressions. Due to the deformability of PDMS, measured pressure drops tend to be smaller than those predicted by the rigid channel geometries (plate and rectangular). Modification of the rigid channel theories with a deformability parameter α provides good fits to the measured data. The elastic plate expression (Eq. (7)) developed by Gervais *et al.*[1] works well for large aspect ratio channels but breaks down when the aspect ratio reaches unity. The elastic rectangular expression (Eq. (10)) developed in this paper does not have a geometric restriction and is better suited for channels with aspect ratio near unity. Based on the fitted α values, we see a consistent trend of decreasing α for smaller width channels, since there is less channel wall to deform. The work presented here will benefit those interested in adding pressure drop measurements in PDMS based microchannels without having to modify existing channel designs or requiring additional fabrication steps.

ACKNOWLEDGMENTS

We gratefully acknowledge support from National Science Foundation CBET-CAREER 0852471 and NSF-DMR 0907638. We also thank Paul Wallace for his help with the microfabrication at the UW Nanotech User Facility.

[1]T. Gervais, J. El-Ali, A. Gunther, and K. F. Jensen, Lab Chip **6**, 500 (2006).
[2]I. Papautsky, T. Ameel, and A. B. Frazier, *ASME International Mechanical Engineering Congress and Exposition*, New York, NY, 1–9 November 2001.
[3]B. J. Adzima and S. S. Velankar, J. Micromech. Microeng. **16**, 1504 (2006).
[4]V. Labrot, M. Schindler, P. Guillot, A. Collin, and M. Joanicot, Biomicrofluidics **3**, 012804 (2009).
[5]C. J. Pipe and G. H. McKinley, Mech. Res. Commun. **36**, 110 (2009).
[6]K. Chung, H. Lee, and H. Lu, Lab Chip **9**, 3345 (2009).
[7]M. Abkarian, M. Faivre, and H. A. Stone, Proc. Natl. Acad. Sci. U.S.A. **103**, 538 (2006).
[8]B. Z. Yang and Q. Lin, Micromech. Microeng. **16**, 411 (2007).
[9]M. S. N. Oliveira, M. A. Alves, F. T. Pinho, and G. H. McKinley, Exp. Fluids **43**, 437 (2007).
[10]M. Kohl, S. Abdelkhalik, S. Jeter, and D. Sadowski, Sens. Actuators, A **118**, 212 (2005).
[11]D. A. Ateya, A. A. Shah, and S. Z. Hua, Ses. Actuators, A **122**, 235 (2005).
[12]A. Kuoni, R. L. Holzherr, M. Boillat, and N. F. De Rooij, J. Micromech. Microeng. **13**, S103–S107 (2003).
[13]C. Y. Wu, W. H. Liao, and Y. C. Tung, Lab Chip **11**, 1740 (2011).
[14]K. Hosokawa, K. Hanada, and R. Maeda, J. Micromech. Microeng. **12**, 1 (2002).
[15]E. P. Kartalov, G. Maltezos, W. F. Anderson, C. R. Taylor, and A. Scherer, J. Appl. Phys. **102**, 084909 (2007).
[16]W. Y. Chang, C. H. Chu, and Y. C. Lin, IEEE Sens. J. **8**, 495 (2008).
[17]B. S. Hardy, K. Uechi, J. Zhen, and H. P. Kavehpour, Lab Chip **9**, 935 (2009).
[18]N. Ichikawa, N. Hosokawa, and R. Maeda, J. Colloid Interface. Sci. **280**, 155 (2004).
[19]J. D. Tice, H. Song, A. D. Lyon, and R. F. Ismagilov, Langmuir **19**, 9127 (2003).
[20]H. Li and M. G. Olsen, Int. J. Heat Fluid Flow **27**, 123 (2006).
[21]K. Young Won and Y. Jung Yul, J. Micromech. Microeng. **18**, 065015 (2008).
[22]B. Zheng, J. D. Tice, and R. F. Ismagilov, Adv. Mater. **16**, 1365 (2004).
[23]H. Bruus, *Theoretical Microfluidics* (Oxford University Press, New York, 2008).
[24]Y. N. Xia and G. M. Whitesides, Annu. Rev. Mater. Sci. **28**, 153 (1998).
[25]M. L. Sheely, Ind. Eng. Chem. **24**, 1060 (1932).
[26]R. Mukhopadhyay, Anal. Chem. **79**, 3248 (2007).
[27]Y. S. Heo, L. M. Cabrera, J. W. Song, N. Futai, Y. Tung, G. D. Smith, and S. Takayama, Anal. Chem. **79**, 1126 (2007).
[28]K. Khanafer, A. Duprey, M. Schlicht, and R. Berguer, Biomed. Microdevices **11**, 503 (2009).